Macromolecules

pubs.acs.org/Macromolecules Article

High Heat Resistance, Barrier Property, and Low Carbon Emission PET for Sustainable Food Packaging Applications Based on Biobased Functional Monomers

Xiaolong Han, Yifei Zhang, Ruidong Wang, Chunxiao Ren, Chenjing Qu, Xiaohui Niu, Weisheng Xiao, Huaxiang Chen,* and Penggang Yin*

Cite This: *Macromolecules* 2025, 58, 5305−5317 Read Online

ACCESS | Metrics & More | Article Recommendations | Supporting Information

ABSTRACT: PET has a wide range of applications in human life. To address the issues including low glass transition temperature, inadequate oxygen barrier properties, and slight brittleness that limit certain applications of PET, 1,4-cyclohexanedimethanol (CHDM) and isosorbide (IS) were incorporated into the PET main chains using a one-pot two-step method, resulting in the formation of PETGI copolymers. Dynamic mechanical and melt rheological properties revealed that the V-shaped fused ring structure of isosorbide hinders the free movement of the polymer chains, which significantly enhanced the heat resistance of the PETGI copolymers. The glass transition temperature of the PETGI copolymers ranges from 80 to 106 °C. Furthermore, CHDM and IS facilitate the amorphous structure of PETGI, yielding a transparency of 98% and superior toughness, with an elongation at break of 234%. The incorporation of isosorbide markedly increases the molecular chain rigidity of the copolymer while reducing the free volume of the polymer. Time-temperature superposition (TTS) provided insight into the structural influence of different monomers in the molecular chain on the fractional free volume (f_g). As a result of these combined factors, the oxygen barrier performance of the PETGI copolymer containing 40% mol of isosorbide was improved by 41% compared to standard PET. The results of sustainability assessment showed that the equivalent $PETGIE_6C_0I_4$ reduces carbon dioxide emissions by nearly 15.4% compared to PET.

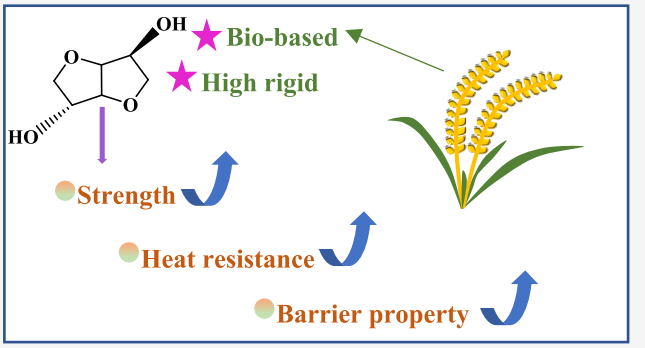

1. INTRODUCTION

A wide range of applications have been developed for poly(ethylene terephthalate) (PET), which represents approximately 18% of the global plastic market.[1] The PET molecular formula shows that the rigid conjugated structure in the chain is formed by direct connection of the rigid benzene ring and the ester groups at both ends. This structure effectively prevents the free rotation of the flexible hydrocarbon group, making PET as a whole show greater rigidity, which means that PET has good wear resistance, heat resistance, corrosion resistance, and dimensional stability. PET has a wide range of applications, such as food and beverage packaging, electronic devices, automotive parts, lighting, sports goods, textiles, healthcare applications, etc.[2] Polyester, one of the three most commonly used synthetic fibers, is produced from PET through spinning and postprocessing. It exhibits excellent performance and is relatively inexpensive.[3]

Nonetheless, there are several shortcomings to consider. PET, for example, is not resistant to hot water cleaning and pasteurization because of its low glass transition temperature (T_g). Furthermore, although the barrier performance of PET is adequate for water (H_2O) and carbon dioxide (CO_2), it exhibits significantly poorer oxygen barrier properties. Most liquors are oxygen-sensitive, so these limitations make PET unsuitable.[4] Several strategies are developed to improve the performance of PET for various applications, in which the most effective way so far is to introduce functional monomers into the molecular structure. For example, to make PET more heat-resistant, the rigid terephthalic acid unit can be replaced with the more rigid 2,6-naphthalene dicarboxylic acid (2,6-N) to give the molecular chain extremely strong rigidity to obtain heat resistance, which provides an idea for the synthesis of polyethylene naphthalate (PEN). However, the cost, limited availability, and environmental considerations narrow the use of 2,6-N to very high-value, low-volume applications such as high-end packaging, films, and fibers. Therefore, the costly PEN is not enough to be a

Received: October 23, 2024
Revised: April 15, 2025
Accepted: May 5, 2025
Published: May 15, 2025

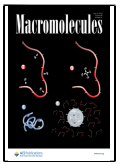

https://doi.org/10.1021/acs.macromol.4c02610
Macromolecules 2025, 58, 5305−5317

Scheme 1. Synthesis Route of PETGI Copolymers

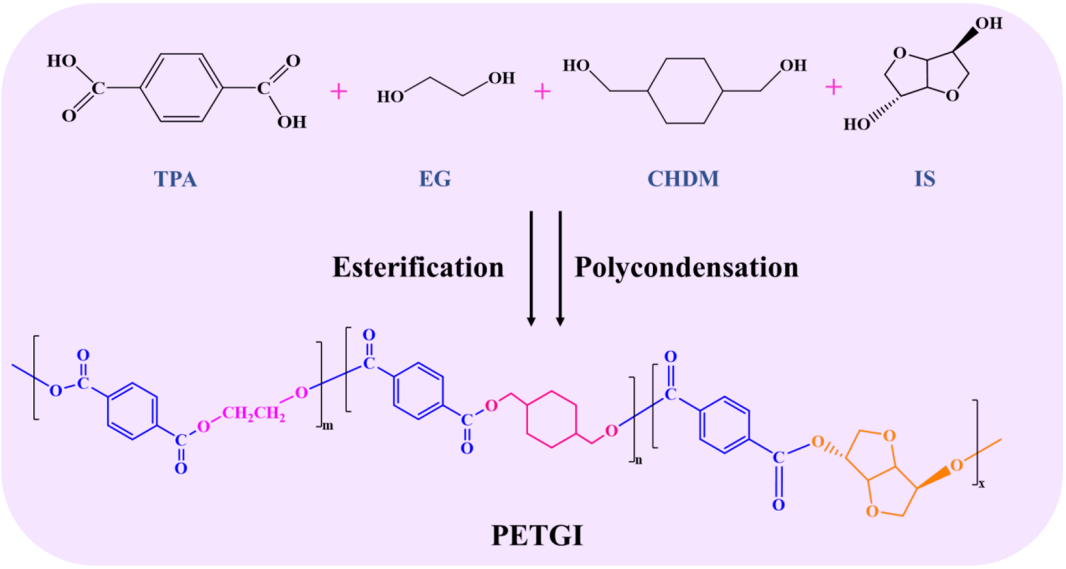

substitute for the widely used PET in life; therefore, it is necessary to find other rigid monomers. Moreover, the brittleness of PET is also one of the important factors limiting its application. To improve the impact resistance and wear resistance, 1,4-cyclohexanedimethanol (CHDM) with a stereoscopic six-membered ring can be used to partially replace the ethylene glycol monomer in PET to obtain better performance as poly(ethylene glycol-*co*-1,4-cyclohexanedimethanol terephthalate) (PETG).

The biobased material isosorbide (IS) can be derived from biomass such as wheat, sugar, and corn, making it a promising monomer.[5,6] IS is a diol with a cyclic structure that has been commercialized.[7] It has been shown through numerous studies that isosorbide is an excellent building block for the development of biobased products,[8−10] which could significantly raise the T_g of the copolymers based on PET,[11] PBT,[12] etc. Nevertheless, a notable limitation of IS is its pronounced sensitivity to highly active catalysts. For instance, the employment of such catalysts during the precondensation stage of copolymer synthesis resulted in significant yellowing. This phenomenon has been attributed to the cleavage of the ether bond in isosorbide, leading to the formation of coloring substances. Highly active catalysts are considered to be strong electrophilic reagents that easily induce isosorbide hydrolysis during the reaction.[13] In this study, various catalysts, including tetrabutyl titanate (TBT), lithium acetylacetonate, cesium carbonate, antimony oxide, and antimony acetate, were employed during the experimental phase. Although titanium- and lithium-based catalysts exhibit superior catalytic efficiency, they also exacerbate the extent of side reactions. In contrast, antimony-based catalysts demonstrate relatively lower activity, resulting in a reduced yellowing of the copolymer. Consequently, antimony catalysts were selected for use in this investigation.

In this work, diol monomers CHDM and IS are introduced into the PET molecular chain to facilitate high oxygen barrier performance and to improve the heat resistance and mechanical properties of PETGI copolymers as low-cost and sustainable candidates for high-performance polymers such as PEN. Moreover, introducing biobased monomer IS into PET will have a positive impact on the environment and reduce carbon emissions.

2. EXPERIMENTAL SECTION

2.1. Experimental Materials. Terephthalic acid (TPA) (99.5%) and ethylene glycol (EG) (99.8%) were purchased from Shanghai Huichao New Material Co., Ltd. 1,4-Cyclohexanedimethanol (CHDM) (99.5%) was purchased from Hebei Qianyuan Xinjing Technology Co., Ltd. Isosorbide (IS) (>98%) was purchased from Beijing Xinhengyan Technology Co., Ltd. Antimony trioxide (Sb_2O_3) (99.5%) and antimony acetate ($Sb(CH_3COO)_3$) (>97%) were purchased from Shanghai Macklin Biochemical Technology Co., Ltd.

2.2. Syntheses of PETGI Copolymers. The copolymers were synthesized using a 5 L stainless steel reactor (Beijing Ximalun Technology Co., Ltd.) equipped with a vacuum pump (TRP-12, Beijing Beiyi Youcheng Vacuum Technology Co., Ltd.). In Scheme 1, PETGI polyesters were synthesized by a two-step polycondensation reaction. The first step was esterification of EG/CHDM, EG/CHDM/IS, or EG/IS with TPA using Sb_2O_3 (0.02 mol % to the diacid) as the esterification catalyst. The molar ratio of overall acid (5 mol) to alcohol (6.25 mol) is 1:1.25. $PETGI_{E6C2I2}$, for example, indicates that the proportions of EG, CHDM and IS in the PETGI copolymer are 60%, 20% and 20% respectively.

Upon stirring, the system was heated to 235 °C in 2 h for the esterification reaction in a nitrogen environment. When the water yield reached more than 90% of the theoretical value, it was considered complete. Following the esterification stage, using Sb $(CH_3COO)_3$ (0.015 mol % to the diacid) as the polycondensation catalyst, prepolycondensation was carried out for 15 min by slowly lowering the system's pressure. The system was heated to 265 °C and evacuated to below 100 Pa. A certain value of propeller torque at a fixed speed signals the completion of polycondensation, and the products are discharged into the cooling water, formed into a strip shape, and cut into pellets.

3. CHARACTERIZATION OF PETGI COPOLYMERS

3.1. Structure Characterization. The signals of PETGI copolymers were collected by the attenuated total reflection (ATR) mode of FTIR, and 64 scans were accumulated in the spectral region of 390-4000 cm^{-1} with a spectral resolution of 4 cm^{-1}.

3.2. Intrinsic Viscosity. In an Ubbelohde viscometer with a capillary tube diameter of 0.792 mm used in a water bath at 25 °C, the intrinsic viscosity of the synthesized copolymers was

https://doi.org/10.1021/acs.macromol.4c02610
Macromolecules 2025, 58, 5305−5317

Table 1. Characteristics of PETGI Copolymers with Various IS Contents

samples	$[\eta]$ (dL/g)[a]	M_η (g/mol)[b]	M_n (g/mol)[c]	M_w(g/mol)[c]	DI[c]
$PETGI_{E6C4I0}$	0.87	2.59×10^4	3.44×10^4	7.49×10^4	2.18
$PETGI_{E6C3I1}$	0.89	2.64×10^4	4.88×10^4	1.05×10^5	2.14
$PETGI_{E6C2I2}$	0.75	2.13×10^4	4.95×10^4	1.07×10^5	2.16
$PETGI_{E6C1I3}$	0.68	1.89×10^4	3.56×10^4	8.47×10^4	2.37
$PETGI_{E6C0I4}$	0.57	1.52×10^4	2.87×10^4	7.20×10^4	2.51

[a]$[\eta]$: intrinsic viscosity. [b]M_η : viscosity-average molecular weight. [c]M_n: number-average molecular weight, M_w: weight-average molecular weight, and DI: molecular weight. dispersity.

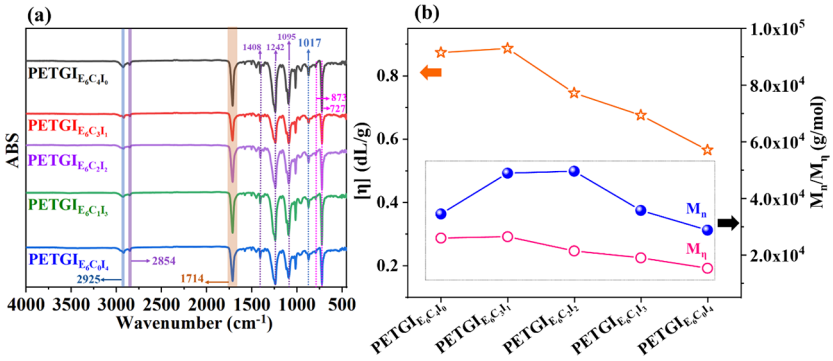

Figure 1. (a) The ATR spectra of PETGI copolymers. (b) The $[\eta]$, M_η, and M_n of PETGI copolymers.

calculated based on the elution time of the copolymer solution and solvent. As a solvent, phenol and tetrachloroethane (1/1, w/w) were mixed, and 0.125 g of the copolymers were used per 25 ml.

3.3. Nuclear Magnetic Resonance (NMR). A Bruker Avance III-400 spectrometer operating at 76.46 MHz and an external static magnetic field of 11.74 T was used to perform solid-state ^{13}C NMR experiments using cross-polarization magic angle spinning (CP/MAS).

3.4. Gel Permeation Chromatography (GPC). A Waters 1515 instrument equipped with a Waters 4.6 × 30 mm guard column and three WAT054466, WAT044226, and WAT044223 columns was used for gel permeation chromatography (GPC), with a differential refractive index detector using trichloromethane (HPLC grade, containing 50 mmol/L LiBr) as the eluent at 35 °C with a flow rate of 1 mL min^{-1}. Polystyrene (PS) standards were used to determine the molecular weights.

3.5. Differential Scanning Calorimetry (DSC). The thermal transitions were recorded with DSC (Discovery 2500, TA, USA) under a N_2 flow of 40 mL min^{-1}. To begin, the sample was heated from 0 to 280°C at 10 °C/min, then held at 280 °C for 2 min, then cooled to 0°C at 10 °C/min, and held for 2 min. As a final step, the sample was heated to 280 °C at 10 °C/min to determine the glass transition temperature (T_g).

3.6. Thermogravimetric Analysis (TGA). The thermal stability of copolymers was assessed using a TGA apparatus (Q-50, TA, USA) with sample weights around 5 mg. The experiments spanned from room temperature to 600 °C at a heating rate of 20 °C/min under a N_2 atmosphere (50 mL/min).

3.7. Optical Property. The optical properties of PETGI copolymers (thickness of 0.3 mm) were characterized on a UV−Vis spectrophotometer (SHIMADZU SolidSpec-3700) in the wavelength interval between 300 and 800 nm.

3.8. Barrier Property. The O_2 barrier properties of PETGI copolymers were studied at 23 °C using GTR-701M. WVTR-9003 was used to measure the water barrier properties of films with a surface area of 38.48 cm^2 prepared by melt-press (thickness: 350−400μm).

3.9. Dynamic Mechanical Property. An analysis of viscoelastic behavior on a dynamic mechanical analyzer (Q800, TA Instruments) was conducted at temperatures ranging from −60 to 200 °C at a heating rate of 3 °C/min and a frequency of 1 Hz.

3.10. Mechanical Property. Synthesized samples were cut into 1.0 mm thick slices and sliced into dumbbell-shaped splines. For each component, at least four samples were tested with a universal testing machine (WDT-10, Kai Power, Shenzhen) at a tensile rate of 10 mm/min.

3.11. Rheological Property. Rheological analysis was conducted on a TA Instruments ARES-G2 using a disposable 25 mm diameter parallel-plate geometry under nitrogen. Strain sweep testing from 0.01 to 10% oscillatory strain at 1 Hz determined the linear viscoelastic region. Using 2% oscillatory strain and a frequency range of 0.1−100 rad/s, frequency sweeps at 10 °C intervals from 190 to 220 °C provided storage and loss moduli and viscosity responses. The TA Instruments TRIOS software shifted the resulting data to generate master curves. The determination of melt flow properties involved fitting the resulting shift factors to the WLF equation in the TRIOS software.

4. RESULTS AND DISCUSSION

4.1. Structural Characterization. We prepared a series of PETGI copolymers as summarized in Table 1, in which *x*, *y*, and *z* of $PETGI_{ExCyIz}$ represented the ratio of EG, CHDM, and ISB in copolymers. For example, $PETGI_{E6C2I2}$ represented the ratio of EG, CHDM, and ISB in copolymers of 60, 20 and 20%, respectively. Meanwhile, $PETGI_{E6C2I2}$ is sometimes referred to as $E_6C_2I_2$ to simplify the expression.

The chemical structures of PETGI copolymers were investigated by FTIR-ATR (Figure 1). The absorption bands at 2925 and 2854 cm^{-1} were the stretching vibration of alkyl C−H. The absorption band at 1714 cm^{-1} was assigned to the

https://doi.org/10.1021/acs.macromol.4c02610
Macromolecules 2025, 58, 5305−5317

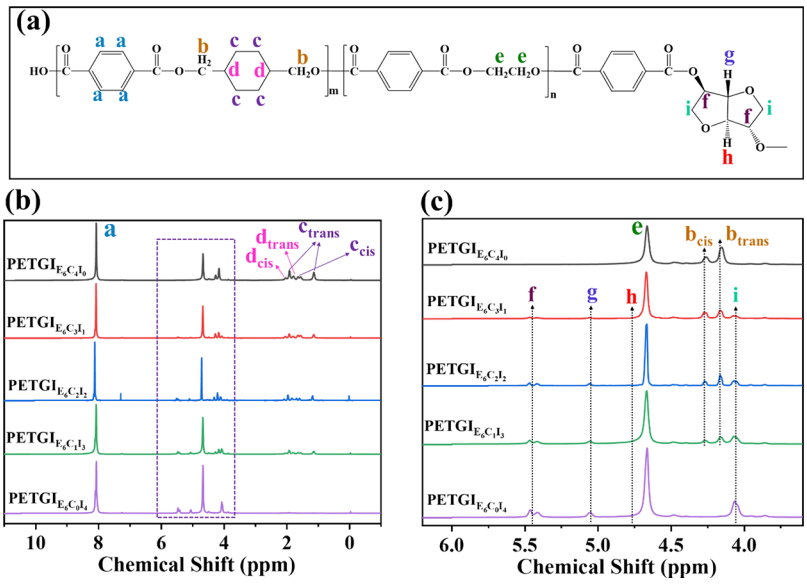

Figure 2. (a) Chain structure of PETGI copolymer. (b) H NMR spectra of PETGI copolymers. (c) Enlargement of chemical shifts **b** (dashed line area).

vibration of the C═O group of the ester group. The absorption bands at 1408, 1242, and 1095 cm^{-1} were assigned to the vibration of C−C on benzene ring. The characteristic band at 1018 cm^{-1} was the vibrational absorption peak of C−O of the ester group in the copolymers. The vibrational absorption peaks of the benzene ring in the fingerprint region were located at 873 and 727 cm^{-1}. The chemical structure of all PETGI copolymers can be determined by infrared spectra, and it is also verified that the target copolymers were successfully obtained by direct esterification.

To determine the molecular weight distribution of all polymers, gel permeation chromatography (GPC) and intrinsic viscosity (IV) were used.

The synthesis route of PETGI copolymers is shown in Scheme 1, and the intrinsic viscosity of the copolymer is shown in Figure 1 b. The M_η of the PETGI copolymers was calculated using the following equations:

$$\eta_r = \frac{t}{t_0} \tag{1}$$

$$\eta_{sp} = \eta_r - 1 \tag{2}$$

$$[\eta] = \frac{1}{c}\sqrt{2(\eta_{sp} - \ln\eta_{sp})} \tag{3}$$

$$[\eta] = KM_\eta^\alpha \tag{4}$$

where t_0 is the elution time of the solvent and t is the elution time of copolymer solutions. In addition, η_r is the relative viscosity, η_{sp} is the specific viscosity, and $[\eta]$ is the intrinsic viscosity. M_η is the viscosity average molecular weight, and K and α are the Mark−Houwink constants that are 0.021 and 0.82, respectively, which could be found and obtained according to the solvent system.[14] The detailed data of PETGI copolymers are listed in Table 1. The $[\eta]$ and M_η of PETGI copolymers range from 0.67 to 0.87 dL/g and 1.52×10^4 to 2.59×10^4 g/mol. The M_η, M_n, and M_w of PETGI copolymers gradually decrease with an increase in the molar ratio of IS, which can be found in Figure 1b and Table 1. Meanwhile, the high content of IS requires a longer polycondensation time to obtain high molecular weights. It is implied that during the copolymerization process, the EG unit and CHDM unit are more prone to chain growth than the IS unit, which is due to the difference in activity between the reactive monomers. The same phenomenon can also be observed from other synthetic works of copolymers containing a biobased monomer (such as isosorbide and 2,5-furandicarboxylic acid).[15−17] As can be seen from the GPC data, the M_n of PETGI copolymers varied from 2.87×10^4 to 4.95×10^4 g/mol. It is worth noting that the introduction of biobased monomers into the copolymer does increase the dispersion of the copolymer, such as IS[17] or FDCA.[18] The DI of the PETGI copolymer is 2.14−2.51, which is a lower dispersity compared to related systems, especially when the IS content is less than 20%.

The structure diagram of PETGI copolymer is shown in Figure 2a. The chemical shift caused by H on the benzene ring appeared at 8.07 ppm, and the methylene absorption peak on ethylene glycol appeared at 4.7 ppm. As shown in the Figure 2b, the chemical shift on 1−2 ppm was H of cyclohexane. The H of isosorbide can be observed at the chemical shift of 4−5.5 ppm in Figure 2c. To determine the molecular structure of the PETGI copolymers, the H NMR results were further analyzed to explore whether the actual ratio of various monomers in the molecular structure unit was close to the feed ratio.

By comparing the areas of resonance absorption peaks produced by the benzene ring, the $-CH_2-$ on both sides of cyclohexane, the $-CH_2-CH_2-$ of ethylene glycol, and the $-CH_2-$ of isosorbide, the actual proportion of CHDM or IS in the whole PETGI copolymers can be accurately calculated. After calculation, the actual content of CHDM is shown in Table 2, which is close to the initial feed ratio and is in line with the experimental expectation. However, the actual content of EG and IS is somewhat different from the initial feeding ratio. However, the actual content of EG and IS is somewhat different from the initial feeding ratio. The reason is because of the low boiling point of ethylene glycol (EG), which is commonly done by adding excess EG to the polyester formulation to compensate for its volatility during the esterification process, as observed in polymers such as PET and PEF. However, as demonstrated in this study, there are significant differences in reactivity between EG, CHDM, and IS during the esterification process. EG has

https://doi.org/10.1021/acs.macromol.4c02610
Macromolecules 2025, 58, 5305−5317

Table 2. Molar Ratios in the Initial Feed and in the Polyester Determined by H NMR

	molar compositions TPA/EG/CHDM/IS	
samples	feed	polyester
$PETGI_{E6C4I0}$	1.00/0.98/0.42/0.00	1.00/0.57/0.37/0.00
$PETGI_{E6C3I1}$	1.00/0.98/0.28/0.14	1.00/0.65/0.25/0.06
$PETGI_{E6C2I2}$	1.00/0.98/0.21/0.21	1.00/0.68/0.20/0.11
$PETGI_{E6C1I3}$	1.00/0.98/0.14/0.28	1.00/0.68/0.14/0.16
$PETGI_{E6C0I4}$	1.00/0.98/0.00/0.40	1.00/0.74/0.00/0.28

higher reactivity than CHDM and IS, and preferential esterification reaction with TPA, resulting in an increase in the loss rate of CHDM and IS, which is also a disadvantage of the one-pot, two-step method. The significantly lowest reactivity of IS leads to its massive loss rate, ranging from 30 to 50%. Finally, most of the unreacted IS, CHDM, and excess EG are removed during the final polycondensation stage.

The ^{13}C NMR spectrum of PETGI copolymers is shown in Figure 3b. The TPA, EG, CHDM, and IS signals have been analyzed and are also marked in Figure 3a. To further characterize the sequence structure of PETGI copolymers, the ^{13}C NMR spectra (132.5−135.5 ppm) was used to investigate the different segment structures of PETGI copolymers in Figure 3c,d.

The ^{13}C NMR spectra (132.5−135.5 ppm) was used to characterize the different segment structures including EG-TPA-EG (ETE), EG-TPA-CHDM (ETC), CHDM-TPA-EG (ETC), CHDM-TPA-CHDM (CTC), IS-TPA-IS (ITI), EG-TPA-IS (ETI), and IS-TPA-EG (ITE) of PETGI copolymers in Figure 3c,d.

The area calculated by the integral of ETE, ETC, CTE, CTC, ITI, ETI, and ITE represented the content of each chain segment in PETGI copolymers.[19] The molar content and average sequence length of ETE, ETC, CTE, CTC, ITI, ETI, and ITE can be calculated by eqs S1−S9, and the random degree R can be calculated by eq 12. The results are shown in Table 3. According to the Bernoullian statistics,[20] it is indicated that PETGI copolymers are all random copolymers and the IS unit is randomly distributed in the molecular chain.

4.4. Thermal Properties of PETGI Polyesters. The DSC curves of PETGI copolymers in Figure 4a indicate a homogeneous amorphous phase in which the glass transition temperature (T_g) value could be estimated. T_g increased with the isosorbide content. The T_g values of $E_6C_3I_1$, $E_6C_2I_2$, and $E_6C_0I_4$ reached 86, 91, and 95 °C, respectively, which were 7, 13.5, and 17.9% higher than that of $E_6C_4I_0$. More importantly, the T_g of $E_6C_0I_4$ reached 106 °C, implying that these copolymers possessed excellent heat resistance. Figure 4c lists the T_g of some common polymers for comparison, and it can be concluded that the heat resistance of PETGI copolymers was only lower than that of PEN and PETGI copolymers can even exceed PEN by further increasing the content of isosorbide. This effect was attributed to the increased chain stiffness from IS with two adjacent furan rings. It is thus possible to tune the thermal behavior of PETGI copolymers to meet the desired performance for a specific application by varying the isosorbide content.

A semiempirical equation, the Gordon−Taylor equation (eq 5), can be fitted to the trend of T_g versus PETGI loading, as

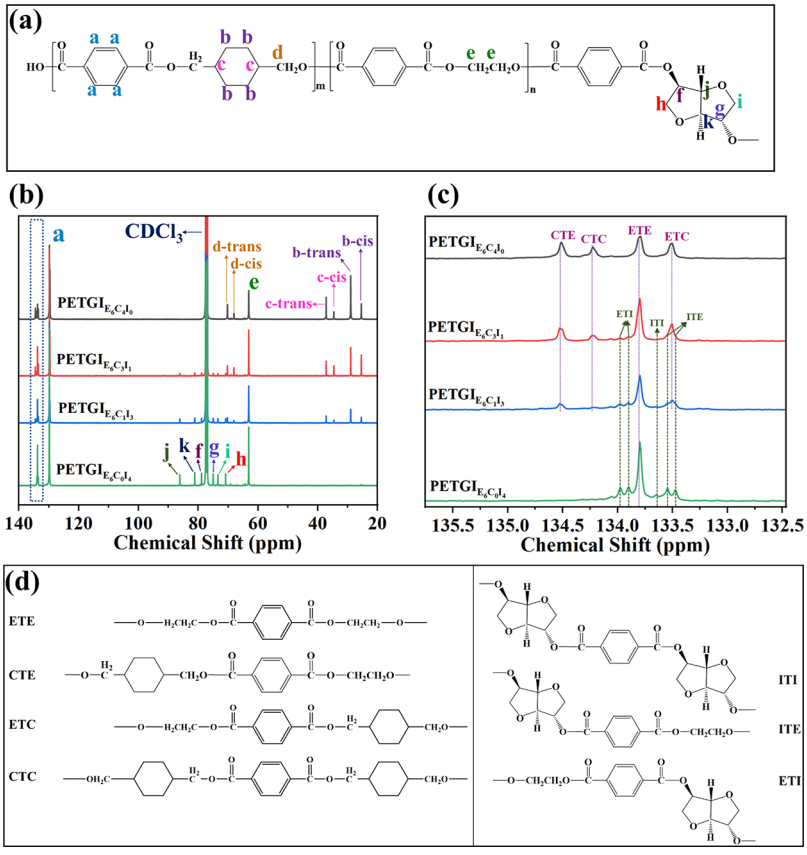

Figure 3. (a) Chain structure of the PETGI copolymer. (b) ^1H NMR spectra of PETGI copolymers. (c) Enlargement of chemical shifts **b** (dashed line area). (d) Schematic diagram of the chain segment structure of PETGI copolymers.

https://doi.org/10.1021/acs.macromol.4c02610
Macromolecules 2025, 58, 5305−5317

Table 3. Molar Fraction, Average Sequence Length, and Degree of Randomness of the PETGI copolymers

	molar fraction (mol %)						average sequence lengths			degree of randomness
sample	N_{ETE}	N_{CTC}	N_{ITI}	$N_{ETC+CTE}$	$N_{ETI+ITE}$	$N_{CTI+ITC}$	n_{ET}	n_{CT}	n_{IT}	R
$PETGI_{E6C4I0}$	32.6	21.1		46.4			2.40	1.90		0.94
$PETGI_{E6C3I1}$	44.6	8.8	0.7	37.6	8.2		2.95	1.47	1.17	1.88
$PETGI_{E6C2I2}$	44.4	6.2	2.2	30.7	16.5		2.88	1.40	1.27	1.85
$PETGI_{E6C1I3}$	44.9	4.5	3.4	25.9	21.3		2.90	1.35	1.32	1.84
$PETGI_{E6C0I4}$	49.0		6.0		45.0		3.17	1.27		1.10

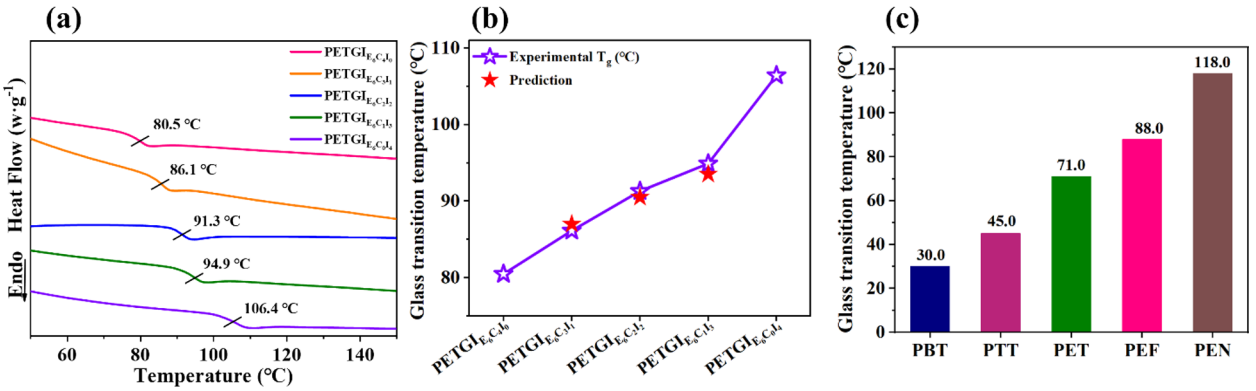

Figure 4. (a) DSC thermograms of PETGI copolymers at a scan rate of 10 °C min^{-1} in the heating process. (b) Comparison of T_g measured by the PETGI copolymer experiment and the predicted values of Gordon−Taylor equation. (c) The T_g of common polymers in life.

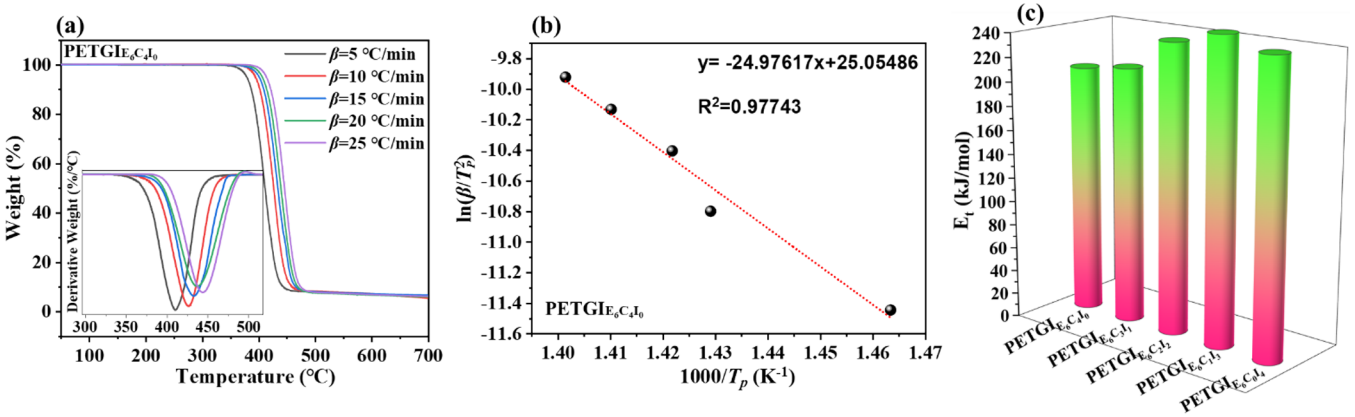

Figure 5. (a) TG-DTG curves of $PETGIE_6C_4I_0$. (b) Kissinger plots of the synthesized $PETGIE_6C_4I_0$. (c) Activation energy (E_t) by the Kissinger method for PETGI copolymers.

Table 4. Thermal Parameters for PETGI Copolymers

sample	(β^a = 10 °C/min) $T_P{}^b$	(β = 10 °C/min) T_P	(β = 15 °C/min) T_P	(β = 20 °C/min) T_P	(β = 25 °C/min) T_P	$E_t{}^c$ (kJ/mol)	R^{2d}
$PETGIE_6C_4I_0$	410.2	426.6	430.2	436.0	440.4	207.7	0.97743
$PETGIE_6C_3I_1$	411.4	426.3	431.0	437.1	440.6	213.2	0.98905
$PETGIE_6C_2I_2$	414.2	426.7	432.9	437.8	439.5	239.8	0.99061
$PETGIE_6C_1I_3$	415.0	429.0	433.4	437.7	439.2	251.0	0.97083
$PETGIE_6C_0I_4$	415.1	429.2	434.4	438.2	440.7	241.3	0.97908

[a]β: heating rate (°C/min). [b]T_P: temperature corresponding to the inflection point (maximum reaction rate) of the thermal degradation curves (°C). [c]E_t: activation energy by Kissinger's method (kJ/mol). [d]R^2: correlation coefficient.

illustrated in Figure 4b. The higher isosorbide loading copolymer can be estimated using the following equation:

$$T_g,\ \text{PETGI polyester} = \frac{k_{GT} w_1 T_{g1} + (1 - w_1) T_{g2}}{k_{GT} w_1 + (1 - w_1)} \quad (5)$$

where T_{g1} and T_{g2} are the T_g of $E_6C_0I_4$ and $E_6C_4I_0$, respectively. w_1 corresponds to the weight fraction of the $E_6C_0I_4$ units in the copolymer, and k_{GT} is the Gordon−Taylor parameter. A highly correlated fit was obtained with $k_{GT} = 2$, indicating behavior that is typical of random copolymers.

4.5. Thermal Stability of PETGI Polyesters. The TGA and derivative thermogravimetry (DTG) curves of PETGI copolymers are shown in Figure 5a and Figure S1. The main thermal parameters are summarized in Table 4, such as the maximum thermal degradation temperature at different heating

https://doi.org/10.1021/acs.macromol.4c02610
Macromolecules 2025, 58, 5305−5317

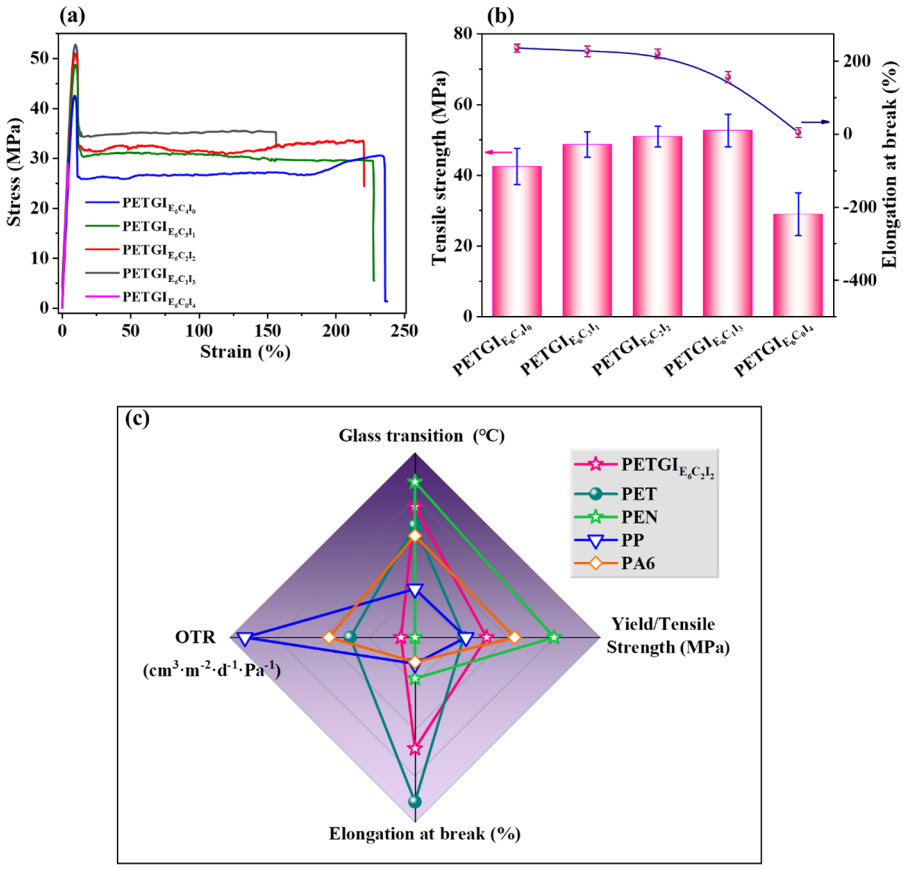

Figure 6. Mechanical properties of PETGI copolymers. (a) Typical stress−train curves. (b) Yield or tensile strength and elongation at break. (c) Comparison of properties of the PETGI copolymer with common polymers.

rates (T_P) and activation energy (E_t). The E_t of PETGI copolymers as shown in Figure 5c can be calculated by various methods. The T_P is analyzed based on Kissinger's method[21] to determine the activation energy from plots of the logarithm of the heating rate versus the inverse of the temperature at the maximum reaction rate in constant heating rate experiments (Figure 5b and Figure S2). The activation energy can be determined by Kissinger's method using the following equation:[22]

$$\ln\left(\frac{\beta}{T_P^2}\right) = -\frac{E_t}{R \cdot T_P} + \text{const} \quad (6)$$

where β is the heating rate, T_p is the temperature corresponding to the inflection point of the thermal degradation curves that correspond to the maximum reaction rate, and R is the gas constant.

In PETGI copolymers, char yields ranged from 10 to 20 wt % remaining, as seen in Figure 5a and Figure S1. It can be seen from TG or DTG curves that the PETGI copolymer had a corresponding mass loss between 350 and 500 °C, which can be attributed to combustion of the organic polymer. The content of IS in PETGI copolymers affected the T_P and E_t of the copolymers. The thermal stability of the PETGI copolymer increases with the increase of IS content. The results showed that the special structure of IS improved the rigidity of the molecular chains and can significantly limit the movement of the molecular chains, which made the polymer chain require higher energy during the pyrolysis process. At the same time, the furan ring of IS forms a large number of intermolecular hydrogen bonds with H atoms of other molecular chains, which improves the molecular chain interaction. The abnormal E_t of C_0I_4 may be caused by the low molecular weight of C_0I_4.

4.6. Mechanical Properties. According to the stress−strain curves, as shown in Figure 6a, the copolymers showed similar yield, plastic deformation, and necking characteristics during ductile deformation, except for $E_6C_0I_4$. $E_6C_0I_4$ showed a brittle performance compared to other copolymers because it did not have a yield point. $E_6C_4I_0$ exhibited high elongation at break and tensile strength (235.93% and 42.52 MPa, respectively) in Figure 6b, and the detailed mechanical parameters of PETGI copolymers are shown in Table S1. With the increase of the ratio of isosorbide in the polymer chain, the tensile strength of the copolymer increased, but the elongation at break decreased gradually. $E_6C_1I_3$ exhibited the highest tensile stress, up to 52.72 MPa. When the amorphous polymer was stretched, unentanglement and orientation of the molecular chains occurred before the polymer was broken. The unentanglement and orientation of the molecular chain were related to the rigidity of the molecular chain. The stronger the molecular chain rigidity was, the worse the unentanglement and orientation ability were, which would decrease the elongation at break of the material.[23] The increase of the ratio of isosorbide in the polymer chain obviously increased the rigidity of the copolymer molecular chain, which can be reflected by a higher glass transition temperature. Therefore, the elongation at break of $E_6C_4I_0$, $E_6C_3I_1$, and $E_6C_2I_2$, $E_6C_1I_3$ copolymers showed a downward trend. But the increase in the rigidity of the polymer chains enabled the materials to withstand higher load without being damaged,[24] which made the yield strength of $E_6C_4I_0$, $E_6C_3I_1$,

https://doi.org/10.1021/acs.macromol.4c02610
Macromolecules 2025, 58, 5305−5317

$E_6C_2I_2$, and $E_6C_1I_3$ copolymers showed an upward trend. On the other hand, the high isosorbide content of C_0I_4 copolymers led to the high rigidity of the molecular chain, which made the material break before yield, so its tensile strength and elongation at break were low. Simultaneously, considering that the high chain stiffness and low molecular weight of C_0I_4 may contribute to its brittle fracture, a comparative experiment was conducted to synthesize C_2I_2 with a reduced molecular weight compared to that of C_0I_4 by adjusting the final polycondensation duration. The characteristics of C_2I_2 (supplementary experiment) are presented in Table S2. The findings indicate that, although C_2I_2 possessed a low molecular weight, it exhibited a yield phenomenon (Figure S3), and its elongation at break reached 97.3%. However, due to its low molecular weight, the tensile strength was approximately 8% lower than that of standard C_2I_2. Consequently, this indirectly substantiated that the brittle fracture of C_0I_4 could be attributed to its high chain stiffness.

4.7. Optical Properties. One of the most important factors in the wide application of polymers is their optical properties. As shown in Figure 7a, $E_6C_4I_0$ was really clear and transparent.

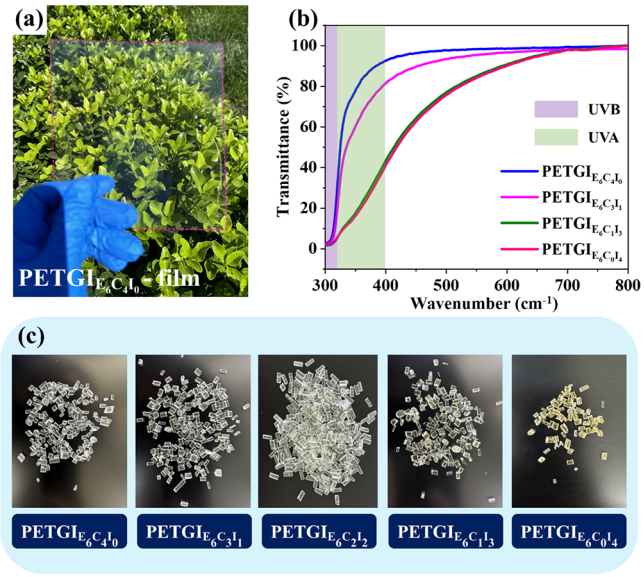

Figure 7. (a) Photographs for $E_6C_4I_0$. (b) UV−visible spectra for PETGI copolymers. (c) Visual picture of copolymers after granulation.

Therefore, the transmittance of 300−800 nm was measured using a UV−visible spectrometer with the curves shown in Figure 7b. For $E_6C_4I_0$, the transmittance was 96% by cutoff 450 nm and 98% by cutoff 700 nm. The increase of isosorbide did not have a significant effect on the transmittance of the copolymers at 700 nm, and it can be clearly observed that the transmittance of all copolymers at 700 nm was about 98%. With the increase of isosorbide units, the transmittance of the copolymers at low wavenumbers decreased obviously, which made the material gradually have the effect of anti-ultraviolet. The reason for this phenomenon may be the breaking of the ether bond in the furan ring of isosorbide in the later stage of the reaction, which led to the yellowing of the material[18] (Figure 7c).

4.8. Dynamic Mechanical Analysis. Figure 8a−d shows the thermomechanical properties characterized by DMA, including the storage modulus (E'), loss modulus (E''), loss angle tangent (tan δ), and complex viscosity plotted as a function of temperature for PETGI copolymers. The storage modulus typically reflects the material's elastic properties. In Figure 8a, all copolymers showed the same curved shapes, indicating that the chain structures of the copolymers were generally the same. The storage modulus of materials decreased slowly with the increase of temperature, but after a certain degree, there will be a sharp reduction. However, the difference is that the higher the proportion of copolymer IS units, the more the curve of the material shifts to high temperature. The complex viscosity (Figure 8d) of PETGI copolymers had the same trend as the curves of the storage modulus, which was due to the molecular chain motion of the polymer. As the chain segments' mobility increased, the modulus decreased sharply with increasing temperature, indicating the beginning of T_g. The copolymers changed from a glassy state to a highly elastic state, and the motion capacities of the chain segments increased greatly, resulting in a sharp decrease in the storage modulus of the copolymers. The higher IS content in the molecular chain caused its storage modulus curve to move to a high temperature, which was because the addition of IS limited the inherent movement ability of the molecular chain. This results in a more rigid molecular chain, making PETGI copolymers with high IS content require higher energy to achieve the same motility ability as low IS content copolymers. The loss modulus of the PETGI copolymers is shown in Figure 8b, where the peak represented the critical point of the two states of the polymer. As the IS content increases, the T_g (measured at the peak of the tan δ curve) of PETGI copolymers continues to increase (Figure 7c), which agreed with the DSC results.

4.9. Barrier Properties. Effective oxygen barrier properties are crucial for packaging materials. Figure 9a shows the oxygen permeability of PETGI copolymers. The oxygen permeability of C_4I_0 without isosorbide was 16.57 $cm^3/m^2{\cdot}24$ h·0.1 MPa. Compared with that, the oxygen permeability of other PETGI copolymers exhibited a trend of decreasing with the increasing content of IS. Among them, the oxygen transmission rate (OTR) of C_0I_4 reached the lowest value of 9.76 $cm^3/m^2{\cdot}24$ h·0.1 MPa, which decreased by 41% compared with C_4I_0.

As illustrated in Figure 9d, there are three steps to the transport of gas molecules through polymer films: adsorption on the high-pressure side, activated diffusion through the film, and desorption on the low-pressure side. The high barrier performances of PETGI copolymers were attributed to the combined action of both chain stiffness increasing[16] and the polar interaction of the furan ring,[25] both of which were caused by the addition of isosorbide into the molecular chain. The polar interaction of the IS furan ring inhibited the adsorption of oxygen on the high-pressure side, thereby providing better barrier properties for the copolymer during "Step 1". The gas permeability of polymers is influenced by their diffusion and solubility processes. Activated diffusion occurs when oscillations of polymer chain segments create void spaces, followed by the translational motion of permeant molecules within the void space before segments to their "normal state".[26] Polymer chain segments will be less able to relax and experience deformation because of the increasing chain stiffness due to the incorporation of isosorbide. As a result, permeant access became difficult to form, which improved oxygen barrier properties[16] and provided better barrier properties for the copolymer during "Step 2". Since PETGI copolymers are amorphous polymers (confirmed by DSC), the effect of crystallinity on copolymers can be excluded when considering the barrier principle of PETGI copolymers.

https://doi.org/10.1021/acs.macromol.4c02610
Macromolecules 2025, 58, 5305−5317

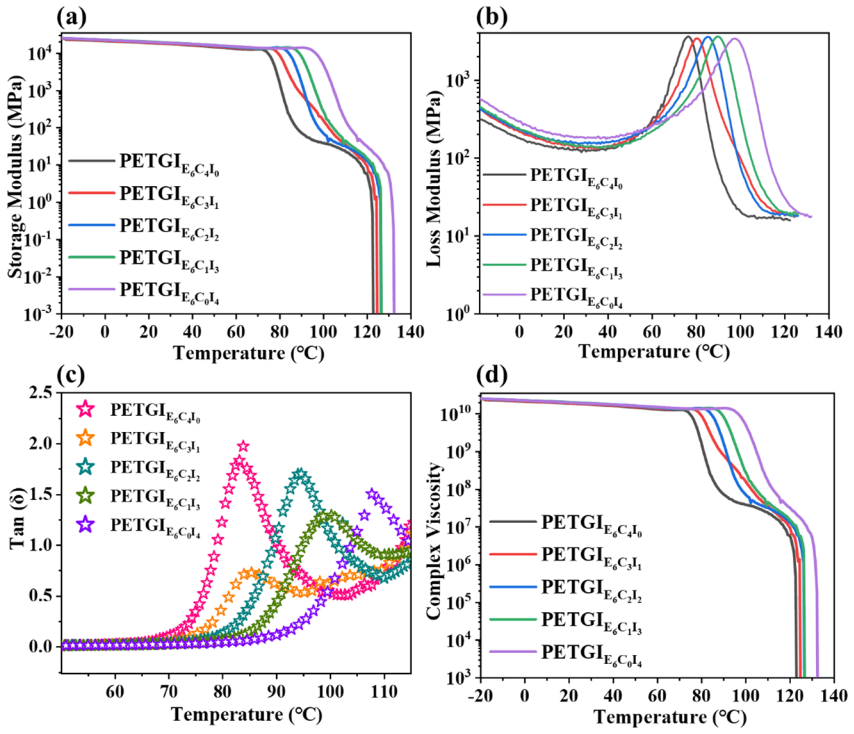

Figure 8. DMA spectra of PETGI copolymers: (a) storage modulus, (b) loss modulus, (c) tan (δ), and (d) complex viscosity.

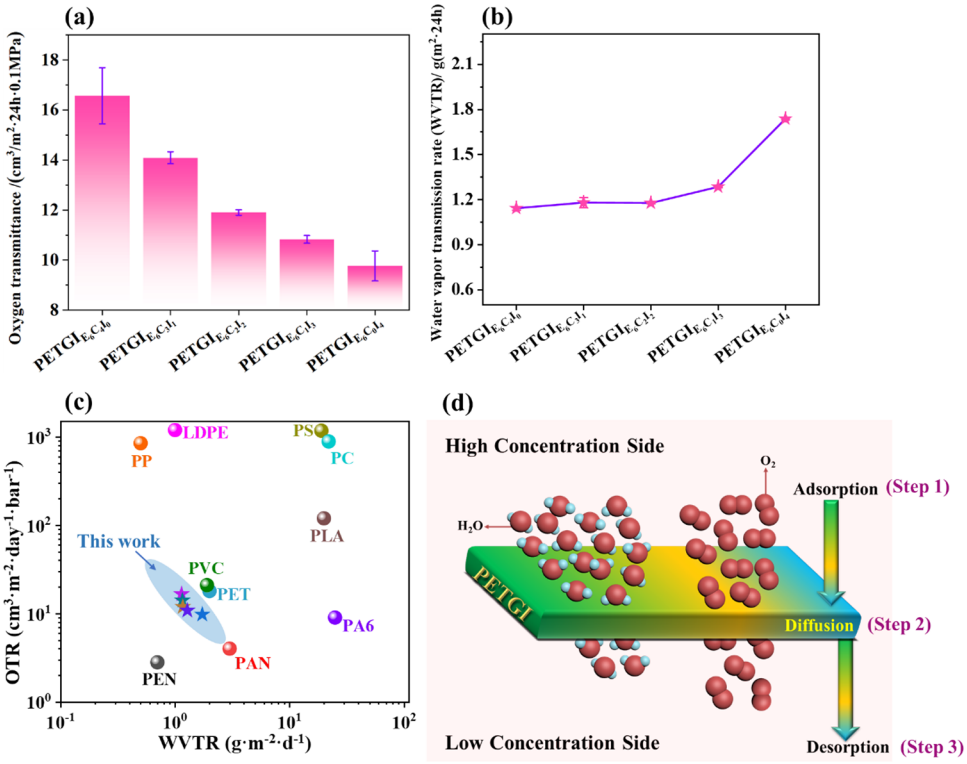

Figure 9. (a) The oxygen transmission of PETGI copolymers. (b) The water vapor transmission of PETGI copolymers. (c) The oxygen and water resistance properties of common polymers[27] and PETGI copolymers. (d) Schematic illustration of permeation through PETGI copolymers.

The water vapor transmittance (WVTR) of PETGI copolymers is shown in Figure 9b. The WVTR of PETGI copolymers exhibited a trend of increasing with the increasing content of IS. In addition to the difficulty of the formation of the permeation access, the characteristics of the isosorbide furan ring should be considered: the oxygen atoms in the furan ring easily bind to water, which increased the adsorption of water on the PETGI copolymers surface. Finally, adsorption on the high-pressure side dominated, and the water resistance of the copolymers deteriorated.

The oxygen and water resistance properties of common polymers are shown in Figure 9c. It can be clearly seen that the

https://doi.org/10.1021/acs.macromol.4c02610
Macromolecules 2025, 58, 5305−5317

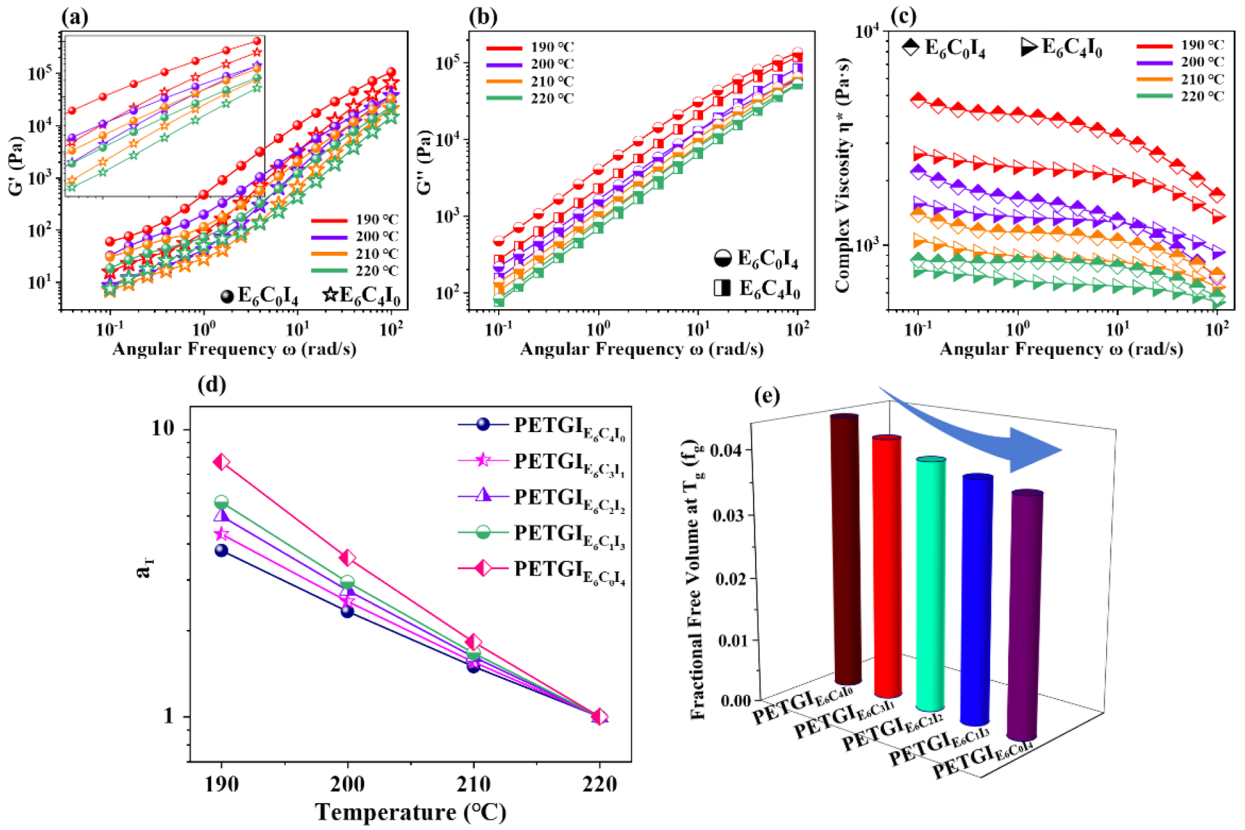

Figure 10. Rheology spectra of PETGI copolymers: (a) storage modulus, (b) loss modulus, and (c) complex viscosity. (d) Representative WLF fitting of shift factors (a_T) versus temperature for PETGI copolymers. T_r = 220 °C. (e) The fractional free volume at T_g (f_g) calculated by the WLF equation.

Table 5. WLF Parameters and Fractional Free Volumes of PETGI Copolymers

sample	T_r	T_g	C_1	C_2 (K)	C_1^g	C_2^g (K)	f_g
$PETGI_{E6C4I0}$	220.0	80.5	3.73	223.50	9.92	84.00	0.0438
$PETGI_{E6C3I1}$	220.0	86.1	3.84	211.21	10.49	77.31	0.0414
$PETGI_{E6C2I2}$	220.0	91.3	3.97	200.50	11.09	71.80	0.0392
$PETGI_{E6C1I3}$	220.0	94.9	4.06	193.32	11.51	68.22	0.0377
$PETGI_{E6C0I4}$	220.0	106.4	4.31	178.57	11.86	64.87	0.0366

barrier properties of PETGI copolymers were obviously better than other polymers and almost equal to PEN, which make PETGI a good candidate as a barrier packaging material.

4.10. Melt Rheology. The influence of the molecular chain rigidity on melt rheological behaviors of PETGI copolymers was investigated with special attention to C_4I_0 and C_0I_4. Figure 10a–c shows the rheological properties including the storage modulus (G'), loss modulus (G''), and complex viscosity (η^*) plotted as a function of angular frequency (ω) for PETGI copolymers at 190, 200, 210, and 220 °C. It can be seen in Figure 10a–c that the G', G'', and η^* of C_0I_4 are higher than those of C_4I_0 at any temperature (the G', G'', and η^* of C_3I_1, C_2I_2, and C_1I_3 are shown in Figure S4). While G', G'', and η^* are indicative of the elastic, viscous, and melt flow properties of the copolymer, respectively, they also reflect the degree of molecular chain rigidity. For instance, at a given temperature, a copolymer with a more rigid molecular chain will exhibit higher values of G' or η^*. This is because a higher storage modulus or viscosity signifies reduced mobility of the copolymer's chain segments, thereby indicating a more rigid molecular chain.

All PETGI copolymers obeyed the Williams–Landel–Ferry (WLF) equation, employing shift factors, a_T, as a function of temperature, as seen in eq 7. The typical behavior for a_T versus temperature by WLF fit is displayed in Figure 10d.

Typical processing temperatures for PETGI copolymers dictated the reference temperature (T_r), and the C_1 and C_2 constants were determined by least-squares regression and were dependent on T_r. By replacing the constants with T_g, C_1^g, and C_2^g, eqs 7–10 enabled us to calculate the fractional free volume at T_g (f_g) as shown in Figure 10e.[28,29]

$$\log(a_T) = \frac{-C_1(T - T_r)}{C_2 + (T - T_r)} \tag{7}$$

$$C_1^g = \frac{C_1 C_2}{C_2 + (T_g - T_r)} \tag{8}$$

$$C_2^g = C_2 + (T_g - T_r) \tag{9}$$

$$f_g = \frac{B}{2.303 C_1^g} \tag{10}$$

Figure 10e shows that increasing the molar ratio of IS in the PETGI copolymer reduced the free volume of the copolymer, which provided a theoretical explanation for the previous

https://doi.org/10.1021/acs.macromol.4c02610
Macromolecules 2025, 58, 5305–5317

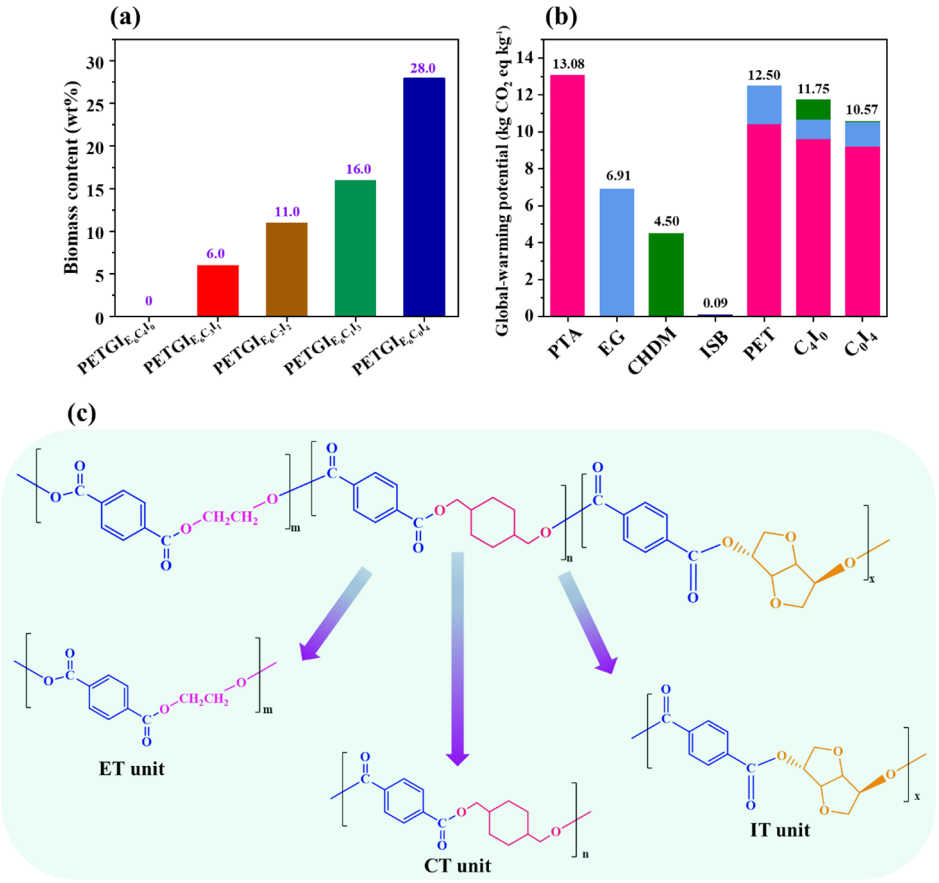

Figure 11. PETGI copolymer environmental friendliness assessment. (a) Biobased content of the series of PETGI copolymers. (b) GWP values of commercial PET, $PETGI_{E6C4I0}$, and $PETGI_{E6C0I4}$. (c) PETGI copolymer molecular formula.

enhancement of the oxygen inhibition capacity of copolymers. Low fractional free volumes of PETGI copolymers indicated the compact packing of chain segments. It could be concluded that the incorporation of isosorbide increased the chain stiffness, which made the polymer chain segments less prone to relaxation and deformation. As a result, permeant access became difficult to form, which improved the oxygen barrier properties (Table 5).

4.11. Sustainability Assessment. LCA serves as a preassessment to determine the positive environmental impact of PETGI copolymer preparation. With the IS ratio increase to 40 mol %, the biobased content in the copolymers increased to 28.0 wt %, as shown in Figure 11a. Contributions from different contents of IS in terms of GWP values were evaluated with the functional unit of 1.0 kg of PETGI copolymers. The contributions of the sources of commercial PET, $PETGI_{E6C4I0}$, and $PETGI_{E6C0I4}$ to total GWP values were assessed. The entire molecular chain of PETGI copolymers can be viewed as a combination of many ET, CT, and IT units (Figure 11c). For Below is an example for $PETGI_{E6C2I2}$:

$$\widehat{M_n} = 0.68 \times M_{nET} + 0.20 \times M_{nCT} + 0.11 \times M_{nIT}$$

$$w_T = \frac{M_{nT}}{\widehat{M_n}} \times 100\%,\ w_E = \frac{M_{nE}}{\widehat{M_n}} \times 100\%,\ w_C = \frac{M_{nC}}{\widehat{M_n}} \times 100\%,\ w_I = \frac{M_{nI}}{\widehat{M_n}} \times 100\% \quad (11)$$

$$\text{raw GWP} = w_T \times GWP_T + w_E \times GWP_E + w_C \times GWP_C + w_I \times GWP_I \quad (12)$$

where GWP_T = 13.08 kg-CO_2-eq,[30] GWP_E = 6.91 kg-CO_2-eq,[17] GWP_C = 4.50 kg-CO_2-eq,[31] GWP_I = 0.09 kg-CO_2-eq.[17] $\widehat{M_n}$ is the average molecular weight of the $PETGI_{E6C2I2}$ segment. M_{nET}, M_{nCT}, and M_{nIT} are the average molecular weights of the ET, CT, and IT unit, respectively. GWP_T, GWP_E, GWP_C, and GWP_I are the GWP values of the raw material for preparing terephthalic acid, ethylene glycol, 1,4-cyclohexanedimethanol, and isosorbide units, respectively. The GWP value of the PETGI raw material part refers to the existing literature. Figure 11b shows the outstanding advantages of $PETGI_{E6C0I4}$ in reducing GWP. Its total GWP value is approximately 10.57 kg-CO_2-eq kg^{-1}, while commercial PET is 12.50 kg-CO_2-eq kg^{-1}. The equivalent $PETGI_{E6C0I4}$ reduces carbon dioxide emissions by nearly 15.4%

https://doi.org/10.1021/acs.macromol.4c02610
Macromolecules 2025, 58, 5305−5317

compared to PET. Due to the use of IS, the potential of PETGI copolymers in sustainable economic development was shown.

5. CONCLUSIONS

A series of isosorbide-based copolymers (PETGI) with good thermal, barrier, and mechanical properties were prepared from renewable raw materials by using a one-pot two-step method. The V-shaped fused ring structure of the isosorbide hinders the free movement of the polymer chains, significantly enhancing the heat resistance of the PETGI copolymers. The glass transition temperature of the PETGI copolymers can be adjusted within the range of 80.48 to 106.43 °C. In addition, the entire series of PETGI copolymers exhibited good mechanical and optical properties. The yield strength of PETGI copolymers ranged from 28.9 to 52.7 MPa, with elongation at break from 235.9 to 4.6%. The visible light transmittance exceeds 90%. Meanwhile, the oxygen resistance of PETGI copolymers with 40% mol isosorbide was 41% higher than that without IS. The total GWP value of PETGI is approximately 10.57 kg-CO_2-eq kg^{-1}, while commercial PET is 12.50 kg-CO_2-eq kg^{-1}. The equivalent $PETGIE_6C_0I_4$ reduces carbon dioxide emissions by nearly 15.4% compared to PET. In summary, PETGI copolymers have the prospect of large-scale production as a green and sustainable material.

■ ASSOCIATED CONTENT

Supporting Information

The Supporting Information is available free of charge at https://pubs.acs.org/doi/10.1021/acs.macromol.4c02610.

Mechanical property parameters for PETGI copolymers; characteristics of $PETGIE_6C_2I_2$ (supplementary experiment); TG-DTG curves of $PETGIE_6C_3I_1$, $PETGIE_6C_2I_2$, $PETGIE_6C_0I_4$, and $PETGIE_6C_1I_3$ based on the Kissinger method; stress−strain curves of $PETGIE_6C_2I_2$ (supplementary experiment); and rheology spectra of PETGI copolymers (PDF)

■ AUTHOR INFORMATION

Corresponding Authors

Huaxiang Chen − *Advanced Materials Research Center, Petrochemical Research Institute, PetroChina Company Limited, Beijing 102206, China*; Email: chenhuaxiang@petrochina.com.cn

Penggang Yin − *Key Laboratory of Bio-Inspired Smart Interfacial Science and Technology of Ministry of Education, School of Chemistry, Beihang University, Beijing 100191, P. R. China*; orcid.org/0000-0001-6796-5921; Email: pgyin@buaa.edu.cn

Authors

Xiaolong Han − *Key Laboratory of Bio-Inspired Smart Interfacial Science and Technology of Ministry of Education, School of Chemistry, Beihang University, Beijing 100191, P. R. China*

Yifei Zhang − *Key Laboratory of Bio-Inspired Smart Interfacial Science and Technology of Ministry of Education, School of Chemistry, Beihang University, Beijing 100191, P. R. China*

Ruidong Wang − *Key Laboratory of Bio-Inspired Smart Interfacial Science and Technology of Ministry of Education, School of Chemistry, Beihang University, Beijing 100191, P. R. China*

Chunxiao Ren − *Advanced Materials Research Center, Petrochemical Research Institute, PetroChina Company Limited, Beijing 102206, China*

Chenjing Qu − *Key Laboratory of Bio-Inspired Smart Interfacial Science and Technology of Ministry of Education, School of Chemistry, Beihang University, Beijing 100191, P. R. China*

Xiaohui Niu − *Advanced Materials Research Center, Petrochemical Research Institute, PetroChina Company Limited, Beijing 102206, China*

Weisheng Xiao − *Advanced Materials Research Center, Petrochemical Research Institute, PetroChina Company Limited, Beijing 102206, China*

Complete contact information is available at: https://pubs.acs.org/10.1021/acs.macromol.4c02610

Notes

The authors declare no competing financial interest.

■ ACKNOWLEDGMENTS

The authors would like to express their acknowledgment to Nan Yang, Beihang University Analysis and Test Center, for the help with DMA analysis. The authors also express their acknowledgment to Maolin Guo, Beijing Technology and Business University, for the help with DSC and optical property analysis.

■ REFERENCES

(1) Eerhart, A.; Faaij, A. P. C.; Patel, M. K. Replacing fossil based PET with biobased PEF; process analysis, energy and GHG balance. *Energy Environ. Sci.* **2012**, *5* (4), 6407−6422.

(2) Shojaei, B.; Abtahi, M.; Najafi, M. Chemical recycling ofPET: A stepping-stone toward sustainability. *Polym. Adv. Technol.* **2020**, *31* (12), 2912−2938.

(3) Sinha, V.; Patel, M. R.; Patel, J. V. Pet Waste Management by Chemical Recycling: A Review. *J. Polym. Environ.* **2010**, *18* (1), 8−25.

(4) Polyakova, A.; Liu, R. Y. F.; Schiraldi, D. A.; Hiltner, A.; Baer, E. Oxygen-barrier properties of copolymers based on ethylene terephthalate. *J. POLYM SCI POL PHYS.* **2001**, *39* (16), 1889−1899.

(5) Saxon, D. J.; Luke, A. M.; Sajjad, H.; Tolman, W. B.; Reineke, T. M. Next-generation polymers: Isosorbide as a renewable alternative. *Prog. Polym. Sci.* **2020**, *101*, No. 101196.

(6) Wang, Y. N.; Wu, J.; Koning, C. E.; Wang, H. P. Short-process synthetic strategies of sustainable isohexide-based polyesters towards higher molecular weight and commercial applicability. *Green Chem.* **2022**, *24* (22), 8637−8670.

(7) Weinland, D. H.; van Putten, R.-J.; Gruter, G.-J. M. Evaluating the commercial application potential of polyesters with 1,4:3,6-dianhydrohexitols (isosorbide, isomannide and isoidide) by reviewing the synthetic challenges in step growth polymerization. *Eur. Polym. J.* **2022**, *164*, No. 110964.

(8) Wang, Y.; Davey, C. J. E.; van der Maas, K.; van Putten, R.-J.; Tietema, A.; Parsons, J. R.; Gruter, G.-J. M. Biodegradability of novel high Tg poly(isosorbide-co-1,6-hexanediol) oxalate polyester in soil and marine environments. *Sci. Total Environ.* **2022**, *815*, No. 152781.

(9) Park, H. S.; Gong, M. S.; Knowles, J. C. Catalyst-free synthesis of high elongation degradable polyurethanes containing varying ratios of isosorbide and polycaprolactone: physical properties and biocompatibility. *J. Mater. Sci. Mater. Med.* **2013**, *24* (2), 281−294.

(10) Wilbon, P. A.; Swartz, J. L.; Meltzer, N. R.; Brutman, J. P.; Hillmyer, M. A.; Wissinger, J. E. Degradable Thermosets Derived from an Isosorbide/Succinic Anhydride Monomer and Glycerol. *ACS Sustain. Chem. Eng.* **2017**, *5* (10), 9185−9190.

(11) Park, S.; Thanakkasaranee, S.; Shin, H.; Ahn, K.; Sadeghi, K.; Lee, Y.; Tak, G.; Seo, J. Preparation and characterization of heat-resistant PET/bio-based polyester blends for hot-filled bottles. *Polym. Test.* **2020**, *91*, No. 106823.

(12) Wang, W.; Wu, F.; Lu, H.; Li, X.; Yang, X.; Tu, Y. A Cascade Polymerization Method for the Property Modification of Poly(butylene terephthalate) by the Incorporation of Isosorbide. *ACS Appl. Polym. Mater.* **2019**, *1* (9), 2313−2321.
(13) Zhang, M.; Lai, W.; Su, L.; Wu, G. Effect of Catalyst on the Molecular Structure and Thermal Properties of Isosorbide Polycarbonates. *Ind. Eng. Chem. Res.* **2018**, *57* (14), 4824−4831.
(14) Zhao, Z. Y.; Wu, Y. Q.; Wang, K. L.; Xia, Y. P.; Gao, H. X.; Luo, K. M.; Cao, Z.; Qi, J. Effect of the Trifunctional Chain Extender on Intrinsic Viscosity, Crystallization Behavior, and Mechanical Properties of Poly(Ethylene Terephthalate). *ACS Omega.* **2020**, *5* (30), 19247−19254.
(15) Hu, H.; Zhang, R.; Jiang, Y.; Shi, L.; Wang, J.; Ying, W. B.; Zhu, J. Toward Biobased, Biodegradable, and Smart Barrier Packaging Material: Modification of Poly(Neopentyl Glycol 2,5-Furandicarboxylate) with Succinic Acid. *ACS Sustain. Chem. Eng.* **2019**, *7* (4), 4255−4265.
(16) Duan, R.; He, Q.-X.; Dong, X.; Li, D.-f.; Wang, X.-l.; Wang, Y.-Z. Renewable Sugar-Based Diols with Different Rigid Structure: Comparable Investigation on Improving Poly(butylene succinate) Performance. *ACS Sustain. Chem. Eng.* **2016**, *4*, 350−362.
(17) Zeng, C.; Ren, J.; Shen, W.; Zhang, S.; Ji, P.; Wang, C.; Wang, H. Synthesis of Thermal-Resistant Polyester-Polycarbonate with Fully Rigid Structure from Biobased Isosorbide. *Macromolecules.* **2024**, *57* (13), 6284−6294.
(18) Shen, A.; Wang, G.; Wang, J.; Zhang, X.; Fei, X.; Fan, L.; Zhu, J.; Liu, X. Poly(1,4-butylene -co-1,4-cyclohexanedimethylene 2,5-furandicarboxylate) copolyester: Potential bio-based engineering plastic. *Eur. Polym. J.* **2021**, *147*, No. 110317.
(19) Xie, S.; Qian, S.; Zhu, K.; Sun, L.; Chen, W.; Chen, S. Comparison of Eco-friendly Ti−M Bimetallic Coordination Catalysts and Commercial Monometallic Sb- or Ti-Based Catalysts for the Synthesis of Poly(ethylene-co-isosorbide terephthalate). *ACS Omega.* **2023**, *8* (22), 19237−19248.
(20) Krimm, S. Polymer sequence determination, carbon-13 NMR method, James C. Randall, Academic, New York, 1977, 155 pp. *J. Polym. Sci.: Polym. Lett. Ed.* **1978**, *16* (9), 481.
(21) Kissinger, H. E. Reaction Kinetics in Differential Thermal Analysis. *Anal. Chem.* **1957**, *29* (11), 1702−1706.
(22) Chrissafis, K.; Paraskevopoulos, K. M.; Bikiaris, D. N. Thermal degradation kinetics of the biodegradable aliphatic polyester, poly(propylene succinate). *Polym. Degrad. Stab.* **2006**, *91* (1), 60−68.
(23) Hong, K.; Rastogi, A.; Strobl, G. A model treating tensile deformation of semicrystalline polymers: Quasi-static stress-strain relationship and viscous stress determined for a sample of polyethylene. *Macromolecules.* **2004**, *37* (26), 10165−10173.
(24) Lee, T. H.; Liu, H. Z.; Forrester, M. J.; Shen, L. Y.; Wang, T. P.; Yu, H. C.; He, J. H.; Li, W. Z.; Kraus, G. A.; Cochran, E. W. Next-Generation High-Performance Biobased Naphthalate-Modified PET for Sustainable Food Packaging Applications. *Macromolecules.* **2022**, *55* (17), 7785−7797.
(25) Genovese, L.; Lotti, N.; Siracusa, V.; Munari, A. Poly(Neopentyl Glycol Furanoate): A Member of the Furan-Based Polyester Family with Smart Barrier Performances for Sustainable Food Packaging Applications. *Materials.* **2017**, *10* (9), 1028.
(26) Miller, K. S.; Krochta, J. M. Oxygen and aroma barrier properties of edible films: A review. *TRENDS FOOD SCI TECH.* **1997**, *8* (7), 228−237.
(27) Huang, H.-D.; Ren, P.-G.; Zhong, G.-J.; Olah, A.; Li, Z.-M.; Baer, E.; Zhu, L. Promising strategies and new opportunities for high barrier polymer packaging films. *Prog. Polym. Sci.* **2023**, *144*, No. 101722.
(28) Mondschein, R. J.; Dennis, J. M.; Liu, H. Y.; Ramakrishnan, R. K.; Nazarenko, S.; Turner, S. R.; Long, T. E. Synthesis and Characterization of Amorphous Bibenzoate (Co)polyesters: Permeability and Rheological Performance. *Macromolecules.* **2017**, *50* (19), 7603−7610.
(29) Mondschein, R. J.; Dennis, J. M.; Liu, H.; Ramakrishnan, R. K.; Sirrine, J. M.; Weiseman, T. F.; Colby, R. H.; Nazarenko, S.; Turner, S. R.; Long, T. E. Influence of Bibenzoate Regioisomers on Cyclohexanedimethanol-Based (Co)polyester Structure−Property Relationships. *Macromolecules.* **2019**, *52* (3), 835−843.
(30) Akanuma, Y.; Selke, S. E. M.; Auras, R. A preliminary LCA case study: comparison of different pathways to produce purified terephthalic acid suitable for synthesis of 100 % bio-based PET. *Int. J. Life Cycle Assess.* **2014**, *19* (6), 1238−1246.
(31) Yuan, L.; Hu, Y.; Zhao, Z.; Li, G.; Wang, A.; Cong, Y.; Wang, F.; Zhang, T.; Li, N. Production of Copolyester Monomers from Plant-Based Acrylate and Acetaldehyde. *Angew. Chem., Int. Ed.* **2022**, *61* (4), No. e202113471.

https://doi.org/10.1021/acs.macromol.4c02610
Macromolecules 2025, 58, 5305−5317